Title: Transcriptome-guided GLP-1 receptor therapy rescues metabolic and behavioral disruptions in a Bardet-Biedl Syndrome mouse model

Authors: Arashdeep Singh[1,2,3*], Naila Haq[4], Mingxin Yang[2,3], Shelby Luckey[3], Samira Mansouri[5], Martha Campbell-Thompson[6], Lei Jin[5], Sofia Christou-Savina[4] and Guillaume de Lartigue[1,2,3*]

Affiliations: [1]Monell Chemical Senses Center, Philadelphia, PA, USA; [2]Department of Neuroscience, University of Pennsylvania, Philadelphia, PA, USA; [3]Department of Pharmacodynamics, College of Pharmacy, University of Florida, USA; [4]Department of Genetics and Genomic Medicine, University College London, UK; [5]Department of Medicine, College of Medicine, University of Florida, USA; [6]Department of Pathology, Immunology and Laboratory Medicine, College of Medicine, University of Florida, USA.

Corresponding Authors and Contact Information:

*Arashdeep Singh and Guillaume de Lartigue

3500 Market Street, Philadelphia, Pennsylvania 19104 USA

Phones: +1-3524103885; +1-4752018057

Emails: singh.arashdeep@hotmail.com; gdelartigue@monell.org

Conflict of Interest: The authors declared no conflict of interest.

Abstract

Bardet-Biedl Syndrome (BBS), a ciliopathy characterized by obesity, hyperphagia, and learning deficits, arises from mutations in *Bbs* genes. More exacerbated symptoms occur with mutations in genes encoding the BBSome, a complex regulating primary cilia function. We investigated the mechanisms underlying BBS-induced obesity using a *Bbs5* knockout (*Bbs5*-/-) mouse model. *Bbs5*-/- mice displayed hyperphagia, learning deficits, glucose/insulin intolerance, and disrupted metabolic hormones, phenocopying human BBS. They displayed an unique immunophenotype in white adipose tissue with increased proinflammatory macrophages and dysfunctional regulatory T cells, suggesting a distinct mechanism for adiposity compared to typical obesity models. Additionally, *Bbs5*-/- mice exhibited pancreatic islet hyperplasia but failed to normalize blood glucose, suggesting defective insulin action. Hypothalamic transcriptomics revealed dysregulated endocrine signaling pathways with functional analyses confirming defects in insulin, leptin, and cholecystokinin (CCK) signalling, while preserving glucagon-like peptide-1 receptor (GLP-1R) responsiveness. Notably, treatment with a GLP-1R agonist effectively alleviated hyperphagia, body weight gain, improved glucose tolerance, and circulating metabolic hormones in *Bbs5*-/- mice. This study establishes *Bbs5*-/- mice as a valuable translational model of BBS to understand the pathogenesis and develop better treatments. Our findings highlight the therapeutic potential of GLP-1R agonists for managing BBS-associated metabolic dysregulation, warranting further investigation for clinical application.

Introduction

Bardet-Biedl Syndrome (BBS) is a rare and debilitating genetic disorder characterized by malfunctions in primary cilia, sensory organelles that play a crucial role in cellular signaling and homeostasis (1). Affecting approximately 1 in 100,000 to 160,000 individuals, BBS presents as a clinically heterogeneous array of symptoms including obesity, learning impairments, retinal dystrophy, and kidney dysfunction (2). The syndrome poses a significant clinical challenge due to its complex genetic etiology, with pathogenic mutations identified in more than 25 genes. These mutations impair the structure and function of cilia, leading to diverse and often severe phenotypic manifestations. Despite substantial advances in genetic and molecular research, effective treatments for BBS remain elusive, largely due to the limited understanding of the underlying pathophysiology.

Central to BBS pathophysiology is the BBSome, a multisubunit protein complex essential for the trafficking of receptors within cilia – a function critical for cellular communication and sensing (3). The BBSome comprises eight core proteins (BBS1, BBS2, BBS4, BBS5, BBS7, BBS8, BBS9, and BBS18), which operate collectively to regulate the transport of receptor molecules within cilia. Disruptions in BBSome assembly or function can impair receptor signaling, leading to the hallmark features of BBS. Among these core components, BBS5 is a compelling target for investigation due to being highly conserved (4) and its critical role in ciliary protein trafficking (2, 5), but remains an understudied component of the BBSome (6). Mutations in *Bbs5* are estimated to account for 2-4% of BBS cases (3, 4). Recent studies suggest that *Bbs*5

mutations lead to disruptions in retinal health (7) and neuronal morphology (8). However, its broader role in physiological and metabolic function remains poorly characterized.

Given that obesity is a hallmark feature of BBS and a significant driver of its associated comorbidities, a deepening understanding of BBS5's role in metabolism could yield critical insights into disease pathogenesis. Our study utilizes *Bbs5* knockout (*Bbs5*-/-) mice as a model to address this knowledge gap by characterizing the physiological impact of BBS5 disruption on cellular and whole-organism metabolism. By elucidating the molecular pathways governed by BBS5, we aim to uncover potential therapeutic targets for treating BBS and related ciliopathies.

Results

Bbs5 knockout mice recapitulate key clinical metabolic dysregulations of BBS. Clinically BBS presents with a high prevalence of early-onset obesity (70-90%) linked to hyperphagia (9). To investigate the specific role of BBS5 in metabolic disease, we employed a *Bbs5*-/- mouse (7) maintained on a homogeneous C57BL/6J background born from heterozygous parents. Although *Bbs5*-/- mice showed no differences in body weight at weaning, they began gaining adiposity at a significantly faster rate after 4 weeks of age, eventually becoming visibly larger than their age-matched wildtype (WT) and heterozygous littermates (Figure 1A). *Bbs5*-/- mice exhibited significant hyperphagia in both light and dark phases compared to WT controls (Figure 1B), leading to increased body weight from 8 weeks of age (Figure 1C) and fat mass

compared to WT littermate controls starting from 6 weeks of age (Figure 1D). Notably lean mass remained comparable between groups (Figure 1E).

In a clinical study, neuropsychological deficiencies including reduced Intelligence Quotient, impaired fine-motor function, social skill deficits, and decreased olfaction, were observed in BBS patients (10). In this study, *Bbs5*-/- mice displayed impaired nest-building behavior (Figure 1F), indicative of potential learning and/or motor deficits. In a novel object recognition paradigm, *Bbs5*-/- mice spent less time exploring the novel object than WT littermates indicative of memory retention deficits (Figure 1G). In an open-field test, *Bbs5*-/- mice exhibited no differences in locomotion (Figure 1H), but they demonstrated reduced center entries (Figure 1I), and time spent in the center (Figure 1J) compared to WT littermates. We observed no additional behavioral disparities in elevated plus maze (Supplementary Figure S1A-B) or Y-maze experiments (Supplementary Figure S1C), suggesting deficits in exploratory behavior without heightened anxiety. Observationally, during feeding experiments, *Bbs5*-/- mice demonstrated a lack of learning to eat from feeders, further supporting the idea of potential learning deficits. Based on our previous findings, we postulate that the behavioral and learning impairments observed in BBS patients could be due to synaptic dysfunction in principal hippocampal neurons (8), however, there is still a need for direct electrophysiological studies to assess synaptic function in *Bbs5*-/- mice.

Consistent with the link to diabetes progression in ciliopathy (11), and higher diabetes prevalence in BBS patients compared to obese controls (12), *Bbs5*-/- mice exhibited

impaired glucose clearance. This was evidenced by elevated circulating glucose levels following glucose administration (Figure 1K) and a higher area under the curve (Figure 1L) compared to WT controls. Similarly, insulin injections failed to reduce circulating glucose levels in *Bbs5*-/- mice (Figure 1M), resulting in a higher area under the curve (Figure 1N). The presence of primary cilia on islet cells is conserved across species (13) and shown to be critical for specific G-protein-coupled receptors signalling to regulate islet insulin and glucagon secretion (14). To elucidate the underlying mechanisms of glucose and insulin intolerance, we conducted a morphological assessment of pancreatic tissue and islet cell architecture in *Bbs5*-/- and WT controls (Figures 1O-V). *Bbs5*-/- mice have similar pancreas size (Figure 1P), but displayed pancreatic islet hyperplasia (Figure 1Q), with a greater percentage of islet area per pancreas (Figure 1R), larger average islet size (Figure 1S-T), and an increased number of insulin cells per islet (Figure 1U). We observed no significant changes in the percentage of insulin cells per proliferating cells between groups (Figure 1V). Consistent with these changes in islet morphology *Bbs5*-/- mice had elevated circulating insulin levels (Figure 2A). Thus, similar to other ciliopathy models (7, 15, 16), ablation of *Bbs5* led to aberrant pancreatic morphology, defective insulin signaling, and impaired glucose homeostasis. These data are consistent with evidence that primary cilia present in insulin-producing β-cells are implicated in regulating glucose metabolism, insulin signaling, and secretion (14, 16, 17).

Importantly, the metabolic and behavioral abnormalities observed in male BBS5-/- mice were recapitulated in females (Supplementary Figure S1D-J), suggesting no sex

differences in disease manifestation. Additionally, neither male (Supplementary Figure S1K-P) nor female (Supplementary Figure S1Q-V) heterozygous *Bbs5*+/- mice displayed any discernable phenotypic changes compared to WT controls. Thus, *Bbs5*-/- mice effectively recapitulate key metabolic and neurobehavioral dysregulation, offering a robust platform for dissecting BBS pathophysiology and developing potential therapeutic strategies.

To better understand the mechanisms underlying the metabolic disruptions in BBS, we investigated changes in a range of metabolic hormones in *ad libitum*-fed wildtype (WT) and *Bbs5*-/- mice. In both male and female mice, *Bbs5*-/- animals exhibited no significant differences in circulating levels of glucagon-like peptide-1 (GLP-1), however, they had elevated circulating levels of insulin, leptin, peptide YY (PYY), C-peptide 2, gastric inhibitory polypeptide (GIP), amylin, and glucagon compared to WT controls (Figure 2A-H). Additionally, no significant differences were observed in circulating pancreatic polypeptide, ghrelin, resistin, and secretin levels (Figure 2I-L). These findings provide a comprehensive endocrine profile of *Bbs5*-/- mice, revealing specific hormonal alterations that may contribute to the metabolic phenotype associated with BBS.

White adipose tissue of Bbs5-/- mice exhibit increased proinflammatory immunophenotype. Primary cilia are highly dynamic organelles that play a vital role in immune (18, 19) and adipocyte function (20, 21). Given the higher fat mass of *Bbs5*-/- mice, we investigated how BBS5 affects adipose tissue immunity in these mice. Evaluation of epididymal white adipose tissue (eWAT) immune cell populations (Figure

3A) revealed no significant differences in total leukocytes and neutrophils compared to controls (Figure 3B-C). However, *Bbs5*-/- mice exhibited a striking increase in eWAT monocytes (Figure 3D). Macrophages, crucial regulators of inflammation (22), were also elevated (Figure 3E). Notably, M2 (anti-inflammatory) were reduced (Figure 3F-G), and M1 (proinflammatory) macrophages were significantly higher (Figure 3H). This shift was recapitulated in female *Bbs5*-/- mice (Supplementary Figure S2B-D). These findings suggest that *Bbs5* mutations disrupt adipose tissue homeostasis by altering immune cells.

Recent studies have implicated regulatory T cells (Tregs), a subset of CD4+ T cells, in promoting anti-inflammatory responses within eWAT (23). Consistent with this, *Bbs5*-/- mice displayed a decrease in total eWAT CD4+ T cells compared to WT controls (Figure 3I). Further analysis revealed a decrease in Gata3+ Th2 cells (Figure 3J), while Rorγt+ Th17 cells were conversely elevated (Figure 3K) but T-bet^{+} Th1 cells were not different compared to WT controls (Figure 3L). Notably, Treg numbers were paradoxically higher in *Bbs5*-/- mice than in WT controls (Figure 3M). However, these Tregs exhibited increased expression of IL17a and Rorγt (Figure 3N-O), markers associated with Th17 cells rather than the immunosuppressive function of Tregs. This dysfunctional Treg phenotype aligns with the chronic, low-grade inflammatory state observed in the eWAT of *Bbs5*-/- mice. Female *Bbs5*-/- mice displayed a similar trend in Treg cell profiles (Supplementary Figure S2E-F).

Bbs5 mutation significantly alters hypothalamic transcriptomics and predicts endocrine dysfunction. To elucidate the molecular underpinnings of BBS-associated hyperphagia and weight gain, we performed bulk RNA sequencing on the hypothalamus of 5-week-old (pre-obesity) and 12-week-old (post-obesity) *Bbs5*-/- mice. Differential gene expression analysis revealed significant alterations in genes associated with primary cilia function at both pre-and post-obesity stages in *Bbs5*-/- mice (Figure 4A and Supplementary Figures S4A, S4B, and S5A). In pre-obese *Bbs5*-/- mice, we found 401 upregulated genes and 549 downregulated genes compared to WT controls (Supplementary Figure S4B). Enriched upregulated gene sets for pre-obese mice were associated with protein sorting and translation, cellular disassembly, RNA transport, DNA and RNA metabolism, and GPCR signalling and the downregulated gene sets included those involved in extracellular structure and hormone metabolic process (Supplementary Figure S4C). In obese *Bbs5*-/- mice, differential expression analysis identified 1539 upregulated genes and 1182 downregulated genes compared to WT controls (Figure 4A). Upregulated gene sets included GPCR signalling, neuropeptide receptor interactions and ligand binding, cilia formation, metabolic processes, and endocrine function Supplementary Figure S5B). Conversely, downregulated gene sets included those related to synaptic regulation, channel activity, mitochondrial function, and enzyme activity (Supplementary Figure S5B).

We observed dysregulation of multiple transcription factors in the hypothalamus, which are critical for various metabolic functions (Figure 4A), including impaired leptin signaling, a hallmark of BBS (24), and disrupted CCK signaling. Based on these

transcriptomic data, we investigated the functional responsiveness of *Bbs5*-/- mice to these satiety hormones (Figure 4B). As expected from previous studies (25), leptin administration significantly reduced food intake and body weight in fasted WT controls (Figure 4C, 4E). However, *Bbs5*-/- mice displayed complete resistance to leptin-induced satiety. This was evident by the absence of change in food intake or body weight following leptin injection (Figure 4D, 4F). This finding aligns with leptin resistance reported in other BBS models (24, 26) and suggests impaired leptin signaling within the hypothalamus of *Bbs5*-/- mice. Importantly, the leptin resistance phenotype was recapitulated in female *Bbs5*-/- mice (Supplementary Figure S3A-D). Interestingly, even heterozygous *Bbs5*+/- mice, which displayed normal body composition and energy metabolism compared to WT controls (Supplementary Figure S1K-V), were resistant to leptin (Supplementary Figure S3K-L, S3O-P), suggesting that leptin resistance may serve as a potential biomarker even in individuals with a single *Bbs* gene mutation.

To further validate the RNA-seq findings we examined the functional responsiveness of *Bbs5*-/- mice to CCK. Consistent with the downregulation of CCK signaling pathway, exogenous CCK administration (2μg or 4μg/kg bodyweight) effectively reduced food intake in fasted WT controls (Figure 4G), demonstrating functional CCK signaling. However, *Bbs5*-/- mice displayed complete resistance to CCK-induced satiety at both doses (Figure 4H-J). This resistance was also observed in female *Bbs5*-/- mice compared to WT controls (Supplementary Figure E-H). Notably, heterozygous *Bbs5*+/- mice responded normally to CCK, indicating intact CCK signaling in this group (Supplementary Figure S3M, S3Q). Thus, as predicted by RNA-seq leptin and CCK

signaling were compromised in *Bbs5*-/- mice which may explain at least part of the hyperphagic phenotype in BBS.

The RNA-seq analysis revealed an unexpected upregulation of numerous hypothalamic satiety hormone receptors, suggesting possible therapeutic targets (Figure 4A). Notably, we observed a 2-3-fold increase in melanocortin-4 receptor (*Mc4r*) and neuropeptide Y2 receptor (*Npy-y2r*) expression in *Bbs5*-/- mice. Interestingly, we found an 8-fold upregulation of glucagon-like peptide-1 receptor (*Glp-1r*). Consistent with the transcriptomic prediction, GLP1R agonist, exendin-4 (0.1,1 and 2µg/kg bodyweight) reduced food intake in both fasted WT and *Bbs5*-/- mice (Figure 4K-L) in a dose-dependent manner (Figure 4M-N). Similar results were also observed in female *Bbs5*-/- mice (Supplementary Figure S3I-J) as well as heterozygous *Bbs5*+/- mice (Supplementary Figure S3N, S3R). These findings suggest that GLP-1R signaling remains functional in *Bbs5*-/- mice and could represent a promising therapeutic target for hyperphagia and obesity associated with BBS.

Glucagon-like peptide-1 receptor agonists improve key clinical metabolic dysregulations in Bbs5-/- mice. GLP-1 receptor agonists (GLP-1RAs), are a class of drugs that have demonstrated efficacy in managing obesity and metabolic disorders. GLP-1RAs, including semaglutide, enhance insulin sensitivity, promote satiety, and reduce body weight (27). Our findings demonstrated elevated hypothalamic GLP-1R expression (Figure 4A) and preserved responsiveness to the acute GLP-1R agonist, Exendin-4, in

Bbs5-/- mice (Figure 4L-N) making them a compelling candidate for addressing BBS-associated metabolic dysfunction.

A crossover design was employed, where mixed-sex *Bbs5*-/- mice received daily subcutaneous injections of vehicle for 14 days followed by semaglutide (0.15mg/kg) for another 14 days (Figure 5A). This dose was chosen based on reported efficacy in preclinical models of obesity (28). Semaglutide treatment significantly decreased daily food intake in *Bbs5*-/- mice, with reductions observed during both the dark and light phases (Figure 5B-C). This translated to a substantial decrease in cumulative food intake over 14 days (Figure 5D). Consequently, *Bbs5*-/- mice treated with semaglutide exhibited rapid weight loss (Figure 5E) and maintained a significant body weight reduction exceeding 10% compared to pre-treatment (Figure 5F). Conversely, during the vehicle treatment arm, *Bbs5*-/- mice trended to gain a small amount of weight (Figure 5F). Semaglutide-induced body weight reduction was accompanied by a decrease in fat mass (Figure 5G), with a smaller decrease in lean mass (Figure 5H). These findings suggest that semaglutide effectively promotes satiety and body weight reduction in *Bbs5*-/- mice.

Beyond its metabolic benefits, semaglutide treatment significantly improved nest-building performance in *Bbs5*-/- mice (Figure 5I). This improvement was accompanied by enhanced glucose clearance, as demonstrated by a lower area under the curve during the intraperitoneal glucose tolerance test (Figure 5J-K). Similar benefits were observed in chow-fed WT mice; however, their nest-building performance was already

at the maximal score, leaving no room for further improvement with semaglutide treatment (Supplementary Figure S6). Treatment with semaglutide, significantly elevated plasma GLP-1 levels in both *Bbs5*-/- and WT mice (Figure 6A), confirming effective intervention regardless of genotypes. In *Bbs5*-/- mice, semaglutide administration led to significant reductions in circulating plasma levels of insulin, leptin, PYY, C-peptide 2, GIP, and amylin (Figure 6B-G) that in many cases normalized the hormonal levels to those of WT littermates. No differences were observed in plasma levels of glucagon, pancreatic polypeptide, ghrelin, resistin, and secretin in *Bbs5*-/- mice before or after semaglutide treatment (Figure 6H-L). Notably, semaglutide treatment did not affect the plasma concentrations of these metabolic hormones in healthy WT mice (Figure 6B-L). These findings suggest GLP-1R agonists hold promise for treating BBS and warrant further clinical investigation.

Discussion

This study establishes *Bbs5*-/- mice as a valuable model for BBS, recapitulating cardinal metabolic and neurobehavioral symptoms observed in patients. We demonstrate that *Bbs5* mutation disrupts energy homeostasis through impaired central nervous system processing of peripheral satiety cues, potentially involving disruptions in adipose tissue and pancreatic function. Elevated levels of key hormones observed in untreated *Bbs5*-/- mice reflect significant metabolic disruptions consistent with insulin resistance, hyperleptinemia, and altered satiety signaling. These findings align with phenotypes commonly associated with BBS, including obesity and metabolic dysregulation.

By integrating behavioral phenotyping with hypothalamic transcriptomics, we identified dysregulated leptin and CCK signaling pathways, central to energy homeostasis. Supporting the relevance of our model, a recent study using stem cell-derived hypothalamic arcuate-like neurons with induced BBS mutations have similarly reported impairments in leptin and insulin signalling (29), underscoring the role of primary cilia in energy homeostasis. Importantly, the observed gene expression changes in *Bbs5*-/- mice are not observed in replicated by prolonged high-fat diet exposure or obesity (30), suggesting that the effects are due to *Bbs5* knockout rather than a secondary response to the metabolic changes. Impaired leptin receptor signaling is a primary mechanism driving weight gain (24, 26) and the role of CCK-A receptor signaling in satiety is well-established (31). Evidence also supports a broader role for CCK-B receptors in modulating feeding behaviors, particularly in stress- or anxiety-related contexts. Prior studies demonstrated that selective antagonism of brain CCK-B receptors increases food intake and delays satiety, suggesting the role for CCK-B receptors in postprandial feeding regulation (32). Furthermore, elevated hypothalamic neuropeptide Y (NPY) levels in CCK-B receptor knockout mice have been linked to hyperphagia, increased fat deposition, and obesity (33, 34). Our data of blunted responses to exogenous CCK and downregulated hypothalamic *Cck-b* receptor in *Bbs5*-/- mice, support a model in which impaired CCK signaling contributes to hyperphagia. In pre-obese *Bbs5*-/- mice, significant downregulation of *Lepr* and *Cck* expression suggests that disruptions in leptin and CCK signaling pathways precede weight gain. Hyperphagia in BBS appears to result from multifactorial disruptions, where intrinsic defects in CCK signaling pathways and receptor function are further exaggerated obesity-related resistance to

satiety signals (31). This concept is supported by our findings in obese *Bbs5*-/- mice, which exhibit additional downregulation of *Cck, Cckbr, Stat3,* and *Socs3* expression indicating that impaired leptin and CCK signaling contribute to the hyperphagia observed in BBS. Together, these studies suggest BBS disrupts CNS processing of satiety cues, contributing to hyperphagia and obesity.

While diet-induced obesity models and genetically obese mice share some similarities, they differ significantly in insulin sensitivity and hormonal profiles, highlighting that obesity-induced effects are not equivalent to those driven by genetic predisposition (35). One limitation of our study is the absence of a lean/pair-fed *Bbs5*-/- group, which could have clarified whether the observed effects in ciliopathies are secondary to obesity. However, our findings are consistent with previous studies of other BBSome genetic knockouts (*Bbs2*-/- and *Bbs4*-/-), which demonstrate that dysregulated leptin receptor signaling is a key ciliopathy-mediated disruption contributing to obesity in Bardet-Biedl Syndrome. Importantly, weight-matching through calorie restriction or pair-feeding to lean control body weights does not restore leptin signaling in these other BBS models, resulting in persistent hyperleptinemia and increased fat mass (24, 26). Compared to diet-induced obese models (23, 36, 37), *Bbs5*-/- mice exhibit distinct metabolic and immune characteristics, including rapid weight gain, pronounced immune dysregulation, and accelerated deterioration of glucose homeostasis and pancreatic function. While both models share hormonal changes and satiety impairments, *Bbs5*-/- mice display a unique immune profile characterized by elevated macrophages, a skewed M1/M2 balance, and regulatory T cells (Tregs) with Th17-like phenotypes, resulting in a pro-

inflammatory signature. These findings underscore disrupted adipose tissue homeostasis in *Bbs5*-/- mice, distinguishing them from diet-induced obesity models and emphasizing the importance of ciliopathy-specific mechanisms in metabolic dysfunction. Furthermore, primary cilia have been reported to cause changes in glucose homeostasis and insulin secretion in islet cells independently of body weight changes (16, 38, 39). This supports the hypothesis that ciliopathies, such as Bardet-Biedl Syndrome, involve intrinsic defects in leptin and insulin pathways, which are exacerbated,rather than solely caused, by obesity. However, further studies are warranted to determine whether metabolic dysfunctions, such as insulin resistance, are direct consequences of ciliopathy or secondary effects of obesity.

Our findings establish that GLP-1R signaling remains functional in *Bbs5*-/- mice, offering a compelling therapeutic target for Bardet-Biedl Syndrome. This directly challenges the hypothesis by Shoemaker et al. (40) that GLP-1R agonists may be ineffective in reducing appetite and body weight in the BBS population. In our study, treatment with semaglutide, a long-acting GLP-1R agonist, effectively mitigated core symptoms of BBS, including reduced food intake, decreased body weight, and improved glucose tolerance and neurobehavioral function. In *Bbs5*-/- mice, semaglutide normalized endocrine function, which may account for the observed improvements in insulin and leptin sensitivity, reduced pro-inflammatory markers, and restored glucose tolerance. Collectively, these findings support the therapeutic potential of GLP-1R agonists for managing BBS. This is further bolstered by a recent case report documenting significant weight loss in a BBS patient treated with a GLP-1R agonist (41).

Semaglutide exhibits broad metabolic and cognitive benefits that extend beyond weight loss. Prior studies show that semaglutide outperforms calorie restriction in diet-induced obese and pair-fed models, notably reducing pancreatic islet hypertrophy and enhancing beta-cell function (42). Pair-fed studies reveal that, while calorie restriction promotes weight loss it fails to reverse the broader spectrum of metabolic dysfunctions linked to obesity. By contrast, semaglutide has been shown to improve cognitive function, including enhanced memory and learning, in both obese and non-obese rodent models (43). We hypothesize that semaglutide's cognitive benefits are at least partially independent of weight loss, although concurrent metabolic improvements make it difficult to disentangle direct effects from secondary ones. Supporting this notion, Marinho et al. demonstrated that semaglutide produced weight-independent metabolic benefits in pair-fed diet-induced obese models (42). These findings underscore the potential of semaglutide to be an effective treatment option, but given the broad effects, there remains a need to establish optimal dosing regimens to ensure long-term safety and efficacy for pediatric and adult patients.

Our hypothalamic transcriptomics data revealed upregulated receptors, including calcitonin receptor, neuropeptide Y2 receptor, and MC4R, providing insights into the neural mechanisms underlying metabolic dysregulation in *Bbs5*-/- mice. Downregulation of hypothalamic *Foxg1* and *Foxo3* expression may partially explain impaired insulin signalling and glucose homeostasis observed in obese *Bbs5*-/- mice (44). Notably, the MC4R agonist Setmelanotide (IMCIVREE) was recently approved by the FDA to

manage BBS-associated weight gain and is under evaluation for additional therapeutic effects in BBS patients (45, 46). However, hypersensitivity or allergic reactions to current medications, as well as defects in certain BBSome genes that disrupt neuropeptide Y2 receptor trafficking to primary cilia, may limit the effectiveness of these therapies in specific BBS cases (47). Nevertheless, other receptor targets, such as the calcitonin receptor present additional avenues for future targets in BBS that could serve as alternative effective therapeutics. Understanding these mechanisms could inform targeting other aspects of BBS pathophysiology, and similar ciliopathies like Alström syndrome.

Notably, the *Bbs5*-/- (***Bbs5***^{tm1b}) mutation in our mice did not exhibit the increased mortality observed in *Bbs5*-/- (***Bbs5***^{tm1a}) (48) or *Bbs3-/-* (49) or *Bbip10-/-* mice (47), suggesting that the *Bbs5* mutation is not inherently lethal. This is consistent with the fact that there are patients with *Bbs5* mutations who survive into adulthood. However, a previous study using the same *Bbs5*-/- (***Bbs5***^{tm1b}) model reported abnormal retinal function (7) consistent with other BBS rodent models (50). *Bbs5*-/- mice exhibit significant visual impairments due to retinal degeneration, including a complete loss of cone photoreceptor function and reduced rod function, as evidenced by structural abnormalities in the outer nuclear layer and mislocalization of photoreceptor proteins. Importantly, these effects are age-dependent, with retinal degeneration becoming pronounced only after 10 months of age (51). To avoid confounding our results with vision-related impairments, all experiments in this study were performed in younger mice, prior to the onset of severe retinal degeneration. Additionally, data from the MRC

indicate that sex differences may exist, with female mice showing fewer or less severe visual defects compared to males. These findings emphasize the need to account for age and gender differences in experimental designs, and they highlight the limitations of the *Bbs5* knockout model in fully replicating the visual phenotypes observed in human Bardet-Biedl Syndrome. Our study highlights the importance of studying ciliopathies, not only as rare genetic disorders but also as critical contributors to metabolic dysregulation in more prevalent forms of obesity. This is supported by recent evidence demonstrating that metabolic disorders such as type 2 diabetes (15, 52) and diet-induced obesity (30) are associated with downregulation in cilia genes - known to be involved in proliferation, cell cycle control, and cilia motility (1), representing a potentially underexplored mechanism contributing to common obesity.

In conclusion, this work offers insights into the interplay between *Bbs5* deficiency, humoral and immune signaling, and metabolic dysregulation. The data support the development of GLP-1R agonists as a promising therapeutic approach for managing the multifaceted clinical manifestations of BBS.

Methods

Sex as a biological variable. Both male and female mice were examined. Differences between sexes were evaluated to study mechanisms.

Animals. Wild-type C57BL/6J male mice (Jackson Laboratories) and heterozygous *Bbs5*+/- mice that harbor a β-galactosidase (lacZ)-tagged, knockout allele of *Bbs5* in exon 4 and 5 (*Bbs5*$^{tm1b(EUCOMM)Wtsi}$) maintained on a C57BL/6J background (MRC Harwell, UK) were used to produce *Bbs5*-/- mice in the study. Upon arrival, mice were acclimated to housing at 22–24 °C under a 12-h light-dark cycle with *ad libitum* access to irradiated water and a low-fat chow diet (LFD, 3.1 kcal/g, Teklad 2018, Envigo, Somerset, NJ, USA) under pathogen-free conditions in the Animal Research Facility at the University of Florida. While both male and female heterozygous mice were fertile, no litters were produced when the homozygous *Bbs5*-/- mice were mated. All mouse experiments were performed according to the regulations and approvals of the Institutional Animal Care and Use Committee at the University of Florida, protocol number 202110305.

Food intake, body weight and body composition measurements. Food consumption was monitored manually using a weighing scale at the end of the dark period (more active phase) and light period (less active phase). Body weight was recorded between 1000 to 1200 h using a conventional weighing scale, and body composition was measured in the unanesthetized mouse by a quantitative magnetic resonance method using an EchoMRI™ 700 Analyzer (EchoMRI LLC, Houston, TX, USA).

Nesting Behavior Test. For nesting trial, each mouse was placed in the home cage with clean corncob bedding (approximately 150g dry weight) and a single pressed cotton square at the end of the light cycle. Mice were allowed to form the nest and photographs of nest formed after 12 hour and 24 hours were recorded for scoring analyses later. For analyses, at least 2 individuals blinded to the study were provided with the scoring criteria (adapted from (53)) and trained with baseline and example nests.

Novel Object Recognition Test. The novel object recognition (NOR) test was used to assess learning and memory in mice. The task was performed in the same chamber as the open field test. The NOR protocol consisted of three phases: habituation, familiarization, and test sessions. During the habituation session, mice were allowed to freely explore the empty open field for 5 min; 24 h later, each mouse was returned to the arena containing two identical objects placed at symmetrical positions 5 cm from the arena wall and allowed to explore them freely for 10 min. During the familiarization session, most mice reached a minimum exploration total for both objects of 30 s. After a retention interval of 24 h, the mouse was returned to the arena where one of the objects was replaced by a novel object and allowed to explore both the familiar object and the novel object for 10 min. All animal behavior tests were conducted in a room illuminated with standard fluorescent lights and digitally recorded with an overhead digital camera (HD Pro Webcam C920, Logitech, Newark, CA, USA). The analysis was performed using Noldus EthoVision XT videotracking software (Noldus Information Technology, Inc.; Leesburg, VA, USA). Exploration time percent was calculated by dividing the time spent with either a familiar or a novel object by the total exploration time in the arena.

Open Field Test. Prior to starting the mice were handled once a day for at least 5 min, 1 week before testing to reduce stress. The open field apparatus used in this study was a squared arena (41 cm x 41 cm) with walls (Height: 30.5 cm) to prevent the animals from escaping. Two regions are defined in the arena: the center, which accounts for 25% of the total area and the periphery, which accounts for the remaining 75% of the total area. Tests were conducted during the dark phase between 1000-1200 h. Mice were placed in the center of the open field with lights on and then allowed to explore for 5 min. All animal behavior tests were conducted in a room illuminated with standard fluorescent lights and digitally recorded with overhead Logitech HD Pro Webcam C920 digital cameras (Newark, CA, USA) and the analysis was performed using Noldus EthoVision XT videotracking software.

Elevated Plus Maze Test. EPM testing was adapted from reported methods (54). The plus-shaped apparatus was made of painted wood consisting of 2 opposite open arms and closed arms (30 × 5 cm) connected by a central platform (5 × 5 cm), with the arms and platform elevated 60 cm from the floor. To start the test, a naïve mouse was placed at the center of the platform along the axis of the open arms, and the mouse's movements on the maze were recorded for 5 minutes with the overhead Logitech digital camera. The maze surfaces were then cleaned with 70% ethanol solution before the next test mouse. Both EPM and Y-maze tests were conducted in a room illuminated with standard fluorescence lights.

Y- Maze Test. To begin the test, a naïve mouse was placed at one corner of the light side with its head facing away from the opening. The mouse's movements were digitally recorded for 8 minutes with an overhead digital camera (HD Pro Webcam C920, Logitech, Newark, CA, USA). The maze arm surface was cleaned with 70% ethanol solution before the next test mouse.

For each behavioral test, mice in both groups were tested in a randomized order to offset potential test sequence bias. Test parameters were independently scored by 2 to 3 individuals blind to the experimental design. Mice were individually brought from the colony room to the behavioral room for the start of each behavioral test.

Intraperitoneal glucose (IPGTT) and insulin (ITT) tolerance test. For IPGTT, after overnight fasting (~16 h), an IP injection of 50% glucose (Sigma-Aldrich) solution at a dose of 2 g/kg body weight was administered to mice. For ITT, after a short fast (~6 h), an IP injection of insulin (Humalog®, Eli Lilly) at 0.5 IU/kg body weight was administered to mice. Blood glucose concentrations were determined from the tail vein using a hand-held glucometer (OneTouch® UltraMini® glucose meter; LifeScan Inc, Malvern, PA, USA) at 0, 15, 30, 60 and 120 min after glucose or insulin injections.

Immunostaining of Pancreas. Pancreas were dissected from fed *ad libitum* 6 WT and 5 *Bbs5*-/- male mice to assess the number of insulin-producing beta-cells. For tissue collection, following cardiac perfusion with PBS and 4% paraformaldehyde (PFA), the pancreas was removed and fixed in PFA for an additional 16 h at 4°C. Following fixation,

the tissue was washed with PBS and then embedded in paraffin. Pancreas sections (4μm) were cut at 4 levels separated by 150μm each (0, 150, 300, and 450 μm) with two serial sections placed per Superfrost Plus slide at each level. The slides were stained using multiplex immunohistochemistry (mIHC) using methods similar to mIHC described for human islets (55). All steps were performed at room temperature except where noted. All primary antibodies were diluted in antibody diluent (ThermoFisher) except for Ki-67 as described below. Sections were heated at 60°C for 1 h, dewaxed in xylenes, and rehydrated in descending ethanols. Sections were subjected to antigen retrieval using pre-heated citrate buffer (BioGenex) for 20 min in a steamer followed by cooling for 20 min. Endogenous peroxidase and alkaline phosphatase activity was blocked with 3% hydrogen peroxide for 10 min. Sections on the left side were blocked with mouse-on-mouse (M.O.M.) Ig blocking reagent (Vector, PK-2200) made up in diluent for 1 h followed by 5 min in M.O.M. diluent. The rabbit anti-Ki67 antibody (Novus Bio, NB500-170) was diluted in M.O.M. diluent at 1:200 and incubated for 1 hour. To detect Ki67 binding, a biotinylated goat anti-rabbit secondary antibody was used at 1:250 dilution for 30 min followed by the ABC reagent (Vector, AK-5000) for 5 min. Sections on the right side were incubated with Sniper (Biocare, BS966M) for 10 min and rabbit anti-somatostatin (Agilent/Dako A0566) diluted at 1:1000 for 1 hour. To detect SST binding, sections were incubated with goat anti-rabbit HRP conjugate (Biocare, RHRP520). The chromogen DAB was used to detect Ki67 and SST for 1-6 min. Slides were then subjected to a second Citra antigen retrieval for 5 min followed by 15 min cooling. Sections were then blocked with dual endogenous enzyme-blocking reagent (DEEB, Agilent/Dako, S200389-2) (10 min) and Avidin/Biotin/Sniper (Vector, SP-2001) (3 min each) in turn, followed by mouse

anti-glucagon (Abcam, ab10988) (1:1000, 30 min), goat anti-mouse alkaline phosphatase (AP) conjugate (Biocare, MALPH521H) (30 min) and detected using Ferangi blue (Biocare, FB813H) (2 min). Sections were subjected to a third Citra antigen retrieval followed by guinea pig anti-insulin (Agilent/Dako, A0564) (1:1000, 30 min), biotinylated goat anti-guinea pig IgG (Vector, BA-7000) (30 min), and Warp red chromogen (Biocare, WR806) (1 min). Sections were counterstained with hematoxylin (Biocare) at 1:10 for 30 sec followed by air drying and mounting.

Blood collection and hormone analysis. Blood samples were collected 2-3 h after the dark onset from the tail vein of mice that had *ad-libitum* food access. The blood samples were collected in tubes containing ethylenediaminetetraacetic acid (EDTA, 1.5 mg/ml blood), protease inhibitor cocktail (10 µl/ml blood; Sigma-Aldrich, Oakville, ON, Canada) and dipeptidyl peptidase IV inhibitor (DPP-IV inhibitor, 10 µl/ml blood; Millipore Corporation, Temecula, CA, USA) and centrifuged for plasma separation which was stored at -80°C until analysis.

Plasma concentrations of Amylin (active), C-Peptide 2, Ghrelin, glucose-dependent insulinotropic polypeptide (GIP, total), glucagon-like peptide-1 (GLP-1, active), Glucagon, Insulin, Leptin, pancreatic polypeptide (PP), peptide YY (PYY), Resistin and Secretin were measured in duplicate by Eve Technologies Corporation (Calgary, AB, Canada) using a commercially available Mouse Metabolic Hormone 12-Plex Discovery Assay® (Millipore Sigma, Burlington, Massachusetts, USA) according to the manufacturer's protocol on a Luminex™ 200 system (Luminex, Austin, TX, USA). Assay sensitivities of

these markers range from 1.4 – 91.8 pg/mL for the 12-plex. Individual analyte sensitivity values are available in the Millipore Sigma MILLIPLEX® MAP protocol.

Isolation of the stromal-vascular fraction from epididymal white adipose tissue. Stromal vascular fraction was isolated from the visceral adipose tissue as previously described (Figure 3A) (56). Briefly, epididymal white adipose tissue (eWAT) was harvested and weighted. 500 mg of epididymal white adipose tissue (eWAT) explants were digested in 1 ml of DMEM supplemented with 2% fatty acid-free BSA (Sigma-Aldrich, 126575), HEPES (10 mM), Liberase TM (thermolysin medium) (25 µg/ml) (Roche, 05401119001), and DNAse (250 µg/ml) (Roche, 10104159001) for 1 h at 37°C. Digested tissue was filtered through a 150-µm mesh into preheated DMEM containing 2% FBS. Cells were spun down at 4°C, 500g for 10 min. Cell pellets were suspended in 0.5 ml ACK buffer to lyse contaminating erythrocytes. Cells were spun and collected at 2200g for 5min at 4°C. Cells were resuspended in FACS buffer.

Adipose Tissue Immunophenotyping and Flow cytometry: Single-cell suspensions from eWAT samples from mice from both groups and both genders were stained with fluorescent-dye-conjugated antibodies in FACS buffer (PBS containing 2% FBS and 1mM EDTA) (56). For intracellular cytokine or transcription factor staining, cells were fixed and permeabilized with the *Foxp3* staining buffer set (eBioscience, 00-5523-00). Data were acquired on a BD LSRFortessa and analyzed using FlowJo software package (FlowJo, LLC). Cell sorting was performed on the BD FACSAria III flow cytometer and cell sorter. The following flow antibodies were used: anti-mouse CD4 PE/Cy7 (clone GK1.5)

(BioLegend, 100422), anti-mouse IL-17a PE (clone TC11-1810.1) (BioLegend, 506903), anti-mouse CD45 PerCP/Cy5.5 (clone 30-F11) (BioLegend,103131), anti-mouse GATA3 (BioLegend, 653809), anti-mouse/human CD11b PE/Cy7 (clone M1/70) (BioLegend, 101216), anti-mouse/human CD11b Brilliant Violet 605 (clone M1/70) (BioLegend, 101237), anti-mouse inducible NO synthase (iNOS) (Invitrogen, 125920), anti-mouse Foxp3 Pacific Blue (clone MF-14) (BioLegend, 26410), anti-mouse/human Arg1 FITC (R&D Systems, IC5868F), anti-mouse F4/80 PerCP/Cy5.5 (clone BM8) (BioLegend, 123127), anti-mouse MGL2/CD301B (BioLegend, 146807), anti-mouse/human T-bet PE/Cy7 (clone 4B10) (Biolegend, 644824), anti-mouse/human RORγt (APC, clone AFKJS-9) (Invitrogen, 17698882), anti-mouse Ly6G (clone 1A8) (BioLegend, 127613), and PE anti-mouse CD206 (clone C068C2) (BioLegend, 141705).

Core Hypothalamic Tissue Dissection. For RNASeq experiment, core hypothalamic tissues of 5-week-old (pre-obesity) and 12-week-old (3 *Bbs5*-/- and 2 WT littermates per age group) mice were collected using a brain tissue slicer and micro-puncher (Integra-Miltex). Briefly, the head was decapitated by cutting posterior to the ears and a midline skin incision was made caudal to the sagittal suture taking care not to cut through the brain. A small cut was made through the anterior of the skull between the eyes. The parietal bones were carefully tilted to expose the brain with meninges. The brain was freed from the meninges and gently lifted from the skull by curved narrow forceps. It was then placed on a precooled petri dish and transferred onto ice. The brain was placed on a precooled brain slicer and sliced using two blades. The tissue slice was removed and transferred to a sylgard-coated petri dish with ice-cold sterile PBS. A part of the

hypothalamus was isolated using an Integra Miltex disposable biopsy punch. The punched tissue was immediately transferred onto a labelled Eppendorf tube and snap-frozen on dry ice.

Hypothalamic RNA sequencing. The libraries for RNASeq were prepared with KAPA Stranded RNA-Seq Kit (Roche Diagnostics Corporation, Indianapolis, IN, USA). The integrity and quantification of RNA were assessed using 4200 TapeStation Instrument (Agilent Technologies). 250 ng RNA was taken for RNASeq library preparation. Sample libraries were prepared with the NEBNext® Ultra™ Directional RNA Library Prep for Illumina® kit (New England Biolabs, Inc.). The workflow consisted of mRNA enrichment, cDNA generation, and end repair to generate blunt ends, A-tailing, adaptor ligation, and PCR amplification. Sequencing was performed on Illumina Hiseq3000 for a single read 50 runs. *Data Processing*: The quality of Fastq files were checked using fastQC and then the reads were aligned to GRCh38 bt TopHat and Bowtie (57). The BAM files outputted by TopHat were quality-checked by RSeQC (58) and mapped by SAMtools. The reads of the filtered BAM files were counted using featureCounts (59). The processing of RNA sequencing was performed by Dr Adrien Jeanniard (UCLA Scientific Core Services, USA). RNASeq analyses were done by DESeq2 (60), a method for differential analysis of count data, using shrinkage estimation for dispersions and fold changes to improve stability and interpretability of estimates. In brief, normalized counts were calculated by dividing raw read counts by sized factors and fitted to a negative binomial distribution followed by the generalised linear model (GLM) likelihood ratio test (61). Statistical significance (P-values) for differentially expressed genes (DEGs) were first corrected by using the R fdrtool (v.1.2.15) package and then adjusted for multiple testing with the Benjamini–

Hochberg correction. 9300 transcripts were removed as the samples lacked those expressions. Differential expression ratio and log2 fold change (FC) were calculated for each significant gene. Down-regulation was indicated by negative fold change whereas positive values accounted for up-regulations.

Acute Drug Studies. Leptin: Animals were fasted overnight (~12 to 14 h) before receiving an i.p. injection 1 h in the dark period of either 0.1% w/v bovine serum albumin (vehicle) or recombinant murine leptin (2 mg/kg of body weight; R&D Systems, Minneapolis, MN, USA) and monitored for changes in food intake and body weight over 24 h. *Cholecystokinin-8:* Animals were fasted overnight (~12 to 14 h) before receiving an i.p. injection 1 h in the dark period of either 0.1% w/v bovine serum albumin (vehicle) or CCK-8 sulfated (2 or 4 μg/kg of body weight; Tocris Bioscience, Minneapolis, MN, USA) and monitored for changes in food intake and body weight over 24 h. *Exendin-4:* Animals were fasted overnight (~12 to 14 h) before receiving an i.p. injection1 h in the dark period of either 0.1% w/v bovine serum albumin (vehicle) or GLP-1 receptor agonist, exendin-4 (0.1, 1 or 2 μg/kg of body weight; Tocris Bioscience, Minneapolis, MN, USA) and monitored for changes in food intake and body weight over 24 h.

Semaglutide Study. To determine the therapeutic potential of GLP-1R agonist on body composition, food intake, and glucose tolerance, mature animals (18-30 weeks old) were subcutaneously injected with either vehicle (6%v/v DMSO in 0.9% saline) or semaglutide (0.15 mg/kg of body weight; gift from Novo Nordisk, Denmark) in a crossover study design (Figure 5A). Mice were injected with the drugs once daily at the onset of dark period and

fed *ad libitum* for 2 weeks. Animals were monitored for changes in daily food intake and body weight, weekly body composition and biweekly glucose tolerance test.

Statistical analysis. Statistical analysis for the experiments is described in each figure legend and was determined using GraphPad Prism 8.3 software. One-way ANOVA, with or without repeated measures, was used for comparing groups; two-way ANOVA, with or without repeated measures, was used for comparing more than one factor between groups as performed for food intake, fat mass, lean mass, body weight, weight gain, and blood glucose during IPGTT and ITT. Mixed model analysis was used in case there was missing data. The sample size (n) for each experiment is shown in the figure legends and corresponds to the sample derived from the individual mice. Data are presented as mean ± SEM and statistical significance is declared at $P < 0.05$.

Study approval. Experiments on animals were performed in accordance with the Guide for the Care and Use of Laboratory Animals of the NIH (National Academies Press, 2011). All animals were handled according to approved University of Florida Institutional Animal Care and Use Committee protocols (202110305).

Data availability. Data are available in the Supporting Data Values file. RNA sequencing differential fold change data set is in the Supporting Data Values file. All RNA transcriptomics data generated in this manuscript have been deposited in the NCBI's Gene Expression Omnibus (GEO) database (GEO GSE293590).

Author Contributions

AS, and GL conceived the study design. AS and GL secured funding. AS, NH, MY, SL, SM, and MCT performed the experiments. AS, NH, MY, SM and GL analyzed the data and AS and GL wrote the manuscript. All authors reviewed and edited the manuscript and had final approval of the submitted version.

Acknowledgments

This study was supported by NIH grants R01 DK116004 (G.L.), R01 DK094871 (G.L.), start-up funds (G.L.), AHA postdoctoral fellowship 23POST1026084 (A. S). The authors thank Novo Nordisk for the provision of semaglutide for the study. The images used for the graphical abstract and in Figures 3A and 4B were created using BioRender.com.

References

1. Nachury MV, Mick DU. Establishing and regulating the composition of cilia for signal transduction. Nat Rev Mol Cell Biol. 2019;20(7):389-405.
2. Tomlinson JW. Bardet-Biedl syndrome: A focus on genetics, mechanisms and metabolic dysfunction. Diabetes Obes Metab. 2024;26 Suppl 2:13-24.
3. Khan SA, Muhammad N, Khan MA, Kamal A, Rehman ZU, Khan S. Genetics of human Bardet–Biedl syndrome, an updates. Clinical Genetics. 2016;90(1):3-15.
4. Li JB, Gerdes JM, Haycraft CJ, Fan Y, Teslovich TM, May-Simera H, et al. Comparative genomics identifies a flagellar and basal body proteome that includes the BBS5 human disease gene. Cell. 2004;117(4):541-52.
5. Nachury MV, Loktev AV, Zhang Q, Westlake CJ, Peränen J, Merdes A, et al. A core complex of BBS proteins cooperates with the GTPase Rab8 to promote ciliary membrane biogenesis. Cell. 2007;129(6):1201-13.
6. Blaess S, Wachten D. The BBSome: a nexus controlling energy metabolism in the brain. The Journal of Clinical Investigation. 2021;131(8).
7. Meehan TF, Conte N, West DB, Jacobsen JO, Mason J, Warren J, et al. Disease model discovery from 3,328 gene knockouts by The International Mouse Phenotyping Consortium. Nature Genetics. 2017;49(8):1231-8.
8. Haq N, Schmidt-Hieber C, Sialana FJ, Ciani L, Heller JP, Stewart M, et al. Loss of Bardet-Biedl syndrome proteins causes synaptic aberrations in principal neurons. PLOS Biology. 2019;17(9):e3000414.
9. Sherafat-Kazemzadeh R, Ivey L, Kahn SR, Sapp JC, Hicks MD, Kim RC, et al. Hyperphagia among patients with Bardet-Biedl syndrome. Pediatric Obesity. 2013;8(5):e64-e7.
10. Brinckman DD, Keppler-Noreuil KM, Blumhorst C, Biesecker LG, Sapp JC, Johnston JJ, et al. Cognitive, sensory, and psychosocial characteristics in patients with Bardet-Biedl syndrome. Am J Med Genet A. 2013;161a(12):2964-71.
11. Hearn T. ALMS1 and Alström syndrome: a recessive form of metabolic, neurosensory and cardiac deficits. J Mol Med (Berl). 2019;97(1):1-17.
12. Volta F, Gerdes JM. The role of primary cilia in obesity and diabetes. Ann N Y Acad Sci. 2017;1391(1):71-84.
13. Cano DA, Murcia NS, Pazour GJ, Hebrok M. Orpk mouse model of polycystic kidney disease reveals essential role of primary cilia in pancreatic tissue organization. Development. 2004;131(14):3457-67.
14. Wu CT, Hilgendorf KI, Bevacqua RJ, Hang Y, Demeter J, Kim SK, et al. Discovery of ciliary G protein-coupled receptors regulating pancreatic islet insulin and glucagon secretion. Genes Dev. 2021;35(17-18):1243-55.
15. Idevall-Hagren O, Incedal Nilsson C, Sanchez G. Keeping pace: the primary cilium as the conducting baton of the islet. Diabetologia. 2024;67(5):773-82.
16. Hughes JW, Cho JH, Conway HE, DiGruccio MR, Ng XW, Roseman HF, et al. Primary cilia control glucose homeostasis via islet paracrine interactions. Proc Natl Acad Sci U S A. 2020;117(16):8912-23.

17. Volta F, Scerbo MJ, Seelig A, Wagner R, O'Brien N, Gerst F, et al. Glucose homeostasis is regulated by pancreatic β-cell cilia via endosomal EphA-processing. Nat Commun. 2019;10(1):5686.
18. Tsyklauri O, Niederlova V, Forsythe E, Prasai A, Drobek A, Kasparek P, et al. Bardet-Biedl Syndrome ciliopathy is linked to altered hematopoiesis and dysregulated self-tolerance. EMBO Rep. 2021;22(2):e50785.
19. Kanie T, Jackson PK. Connecting autoimmune disease to Bardet-Biedl syndrome and primary cilia. EMBO Rep. 2021;22(2):e52180.
20. Wu Y, Zhou J, Yang Y. Peripheral and central control of obesity by primary cilia. Journal of Genetics and Genomics. 2023;50(5):295-304.
21. Hilgendorf KI. Primary Cilia Are Critical Regulators of White Adipose Tissue Expansion. Front Physiol. 2021;12:769367.
22. Castoldi A, Naffah de Souza C, Câmara NO, Moraes-Vieira PM. The Macrophage Switch in Obesity Development. Front Immunol. 2015;6:637.
23. Deng T, Liu J, Deng Y, Minze L, Xiao X, Wright V, et al. Adipocyte adaptive immunity mediates diet-induced adipose inflammation and insulin resistance by decreasing adipose Treg cells. Nature Communications. 2017;8(1):15725.
24. Seo S, Guo DF, Bugge K, Morgan DA, Rahmouni K, Sheffield VC. Requirement of Bardet-Biedl syndrome proteins for leptin receptor signaling. Hum Mol Genet. 2009;18(7):1323-31.
25. Friedman JM, Halaas JL. Leptin and the regulation of body weight in mammals. Nature. 1998;395(6704):763-70.
26. Rahmouni K, Fath MA, Seo S, Thedens DR, Berry CJ, Weiss R, et al. Leptin resistance contributes to obesity and hypertension in mouse models of Bardet-Biedl syndrome. J Clin Invest. 2008;118(4):1458-67.
27. Drucker DJ. Mechanisms of Action and Therapeutic Application of Glucagon-like Peptide-1. Cell Metab. 2018;27(4):740-56.
28. Gabery S, Salinas CG, Paulsen SJ, Ahnfelt-Rønne J, Alanentalo T, Baquero AF, et al. Semaglutide lowers body weight in rodents via distributed neural pathways. JCI Insight. 2020;5(6).
29. Wang L, Liu Y, Stratigopoulos G, Panigrahi S, Sui L, Zhang Y, et al. Bardet-Biedl syndrome proteins regulate intracellular signaling and neuronal function in patient-specific iPSC-derived neurons. The Journal of Clinical Investigation. 2021;131(8).
30. Deng G, Morselli LL, Wagner VA, Balapattabi K, Sapouckey SA, Knudtson KL, et al. Single-Nucleus RNA Sequencing of the Hypothalamic Arcuate Nucleus of C57BL/6J Mice After Prolonged Diet-Induced Obesity. Hypertension. 2020;76(2):589-97.
31. Kopin AS, Mathes WF, McBride EW, Nguyen M, Al-Haider W, Schmitz F, et al. The cholecystokinin-A receptor mediates inhibition of food intake yet is not essential for the maintenance of body weight. J Clin Invest. 1999;103(3):383-91.
32. Dourish CT, Rycroft W, Iversen SD. Postponement of satiety by blockade of brain cholecystokinin (CCK-B) receptors. Science. 1989;245(4925):1509-11.
33. Chen H, Kent S, Morris MJ. Is the CCK2 receptor essential for normal regulation of body weight and adiposity? European Journal of Neuroscience. 2006;24(5):1427-33.
34. Clerc P, Coll Constans MGc, Lulka H, Broussaud Sp, Guigné C, Leung-Theung-Long Sp, et al. Involvement of Cholecystokinin 2 Receptor in Food Intake Regulation: Hyperphagia and

Increased Fat Deposition in Cholecystokinin 2 Receptor-Deficient Mice. Endocrinology. 2007;148(3):1039-49.
35. Lutz TA, Woods SC. Overview of animal models of obesity. Curr Protoc Pharmacol. 2012;Chapter 5:Unit5.61.
36. Winer S, Chan Y, Paltser G, Truong D, Tsui H, Bahrami J, et al. Normalization of obesity-associated insulin resistance through immunotherapy. Nature Medicine. 2009;15(8):921-9.
37. Kiran S, Rakib A, Kodidela S, Kumar S, Singh UP. High-Fat Diet-Induced Dysregulation of Immune Cells Correlates with Macrophage Phenotypes and Chronic Inflammation in Adipose Tissue. Cells. 2022;11(8):1327.
38. Vaisse C, Reiter JF, Berbari NF. Cilia and Obesity. Cold Spring Harb Perspect Biol. 2017;9(7).
39. Cho JH, Li ZA, Zhu L, Muegge BD, Roseman HF, Lee EY, et al. Islet primary cilia motility controls insulin secretion. Science Advances. 2022;8(38):eabq8486.
40. Shoemaker A. Bardet-Biedl syndrome: A clinical overview focusing on diagnosis, outcomes and best-practice management. Diabetes Obes Metab. 2024;26 Suppl 2:25-33.
41. Ganawa S, Santhosh SH, Parry L, Syed AA. Weight loss with glucagon-like peptide-1 receptor agonists in Bardet-Biedl syndrome. Clin Obes. 2022;12(5):e12546.
42. Marinho TS, Martins FF, Cardoso LEM, Aguila MB, Mandarim-de-Lacerda CA. Pancreatic islet cells disarray, apoptosis, and proliferation in obese mice. The role of Semaglutide treatment. Biochimie. 2022;193:126-36.
43. Tipa RO, Balan DG, Georgescu MT, Ignat LA, Vacaroiu IA, Georgescu DE, et al. A Systematic Review of Semaglutide's Influence on Cognitive Function in Preclinical Animal Models and Cell-Line Studies. Int J Mol Sci. 2024;25(9).
44. Lee S, Dong HH. FoxO integration of insulin signaling with glucose and lipid metabolism. J Endocrinol. 2017;233(2):R67-r79.
45. Wang Y, Bernard A, Comblain F, Yue X, Paillart C, Zhang S, et al. Melanocortin 4 receptor signals at the neuronal primary cilium to control food intake and body weight. The Journal of Clinical Investigation. 2021;131(9).
46. Haws R, Brady S, Davis E, Fletty K, Yuan G, Gordon G, et al. Effect of setmelanotide, a melanocortin-4 receptor agonist, on obesity in Bardet-Biedl syndrome. Diabetes Obes Metab. 2020;22(11):2133-40.
47. Loktev AV, Jackson PK. Neuropeptide Y family receptors traffic via the Bardet-Biedl syndrome pathway to signal in neuronal primary cilia. Cell Rep. 2013;5(5):1316-29.
48. Bentley-Ford MR, Engle SE, Clearman KR, Haycraft CJ, Andersen RS, Croyle MJ, et al. A mouse model of BBS identifies developmental and homeostatic effects of BBS5 mutation and identifies novel pituitary abnormalities. Human Molecular Genetics. 2021;30(3-4):234-46.
49. Kawasaki M, Izu Y, Hayata T, Ideno H, Nifuji A, Sheffield VC, et al. Bardet-Biedl syndrome 3 regulates the development of cranial base midline structures. Bone. 2017;101:179-90.
50. Lee H, Song J, Jung JH, Ko HW. Primary cilia in energy balance signaling and metabolic disorder. BMB Rep. 2015;48(12):647-54.
51. Kretschmer V, Patnaik SR, Kretschmer F, Chawda MM, Hernandez-Hernandez V, May-Simera HL. Progressive Characterization of Visual Phenotype in Bardet-Biedl Syndrome Mutant Mice. Investigative Ophthalmology & Visual Science. 2019;60(4):1132-43.

52. Kluth O, Stadion M, Gottmann P, Aga H, Jähnert M, Scherneck S, et al. Decreased Expression of Cilia Genes in Pancreatic Islets as a Risk Factor for Type 2 Diabetes in Mice and Humans. Cell Reports. 2019;26(11):3027-36.e3.
53. Neely CLC, Pedemonte KA, Boggs KN, Flinn JM. Nest Building Behavior as an Early Indicator of Behavioral Deficits in Mice. J Vis Exp. 2019(152).
54. Walf AA, Frye CA. The use of the elevated plus maze as an assay of anxiety-related behavior in rodents. Nat Protoc. 2007;2(2):322-8.
55. Campbell-Thompson M, Fu A, Kaddis JS, Wasserfall C, Schatz DA, Pugliese A, et al. Insulitis and β-Cell Mass in the Natural History of Type 1 Diabetes. Diabetes. 2016;65(3):719-31.
56. Mansouri S, Gogoi H, Patel S, Katikaneni DS, Singh A, Aybar-Torres A, et al. MPYS Modulates Fatty Acid Metabolism and Immune Tolerance at Homeostasis Independent of Type I IFNs. J Immunol. 2022;209(11):2114-32.
57. Trapnell C, Pachter L, Salzberg SL. TopHat: discovering splice junctions with RNA-Seq. Bioinformatics. 2009;25(9):1105-11.
58. Wang L, Wang S, Li W. RSeQC: quality control of RNA-seq experiments. Bioinformatics. 2012;28(16):2184-5.
59. Liao Y, Smyth GK, Shi W. featureCounts: an efficient general purpose program for assigning sequence reads to genomic features. Bioinformatics. 2014;30(7):923-30.
60. Love MI, Huber W, Anders S. Moderated estimation of fold change and dispersion for RNA-seq data with DESeq2. Genome Biology. 2014;15(12):550.
61. McCarthy DJ, Chen Y, Smyth GK. Differential expression analysis of multifactor RNA-Seq experiments with respect to biological variation. Nucleic Acids Res. 2012;40(10):4288-97.

Figures and legends

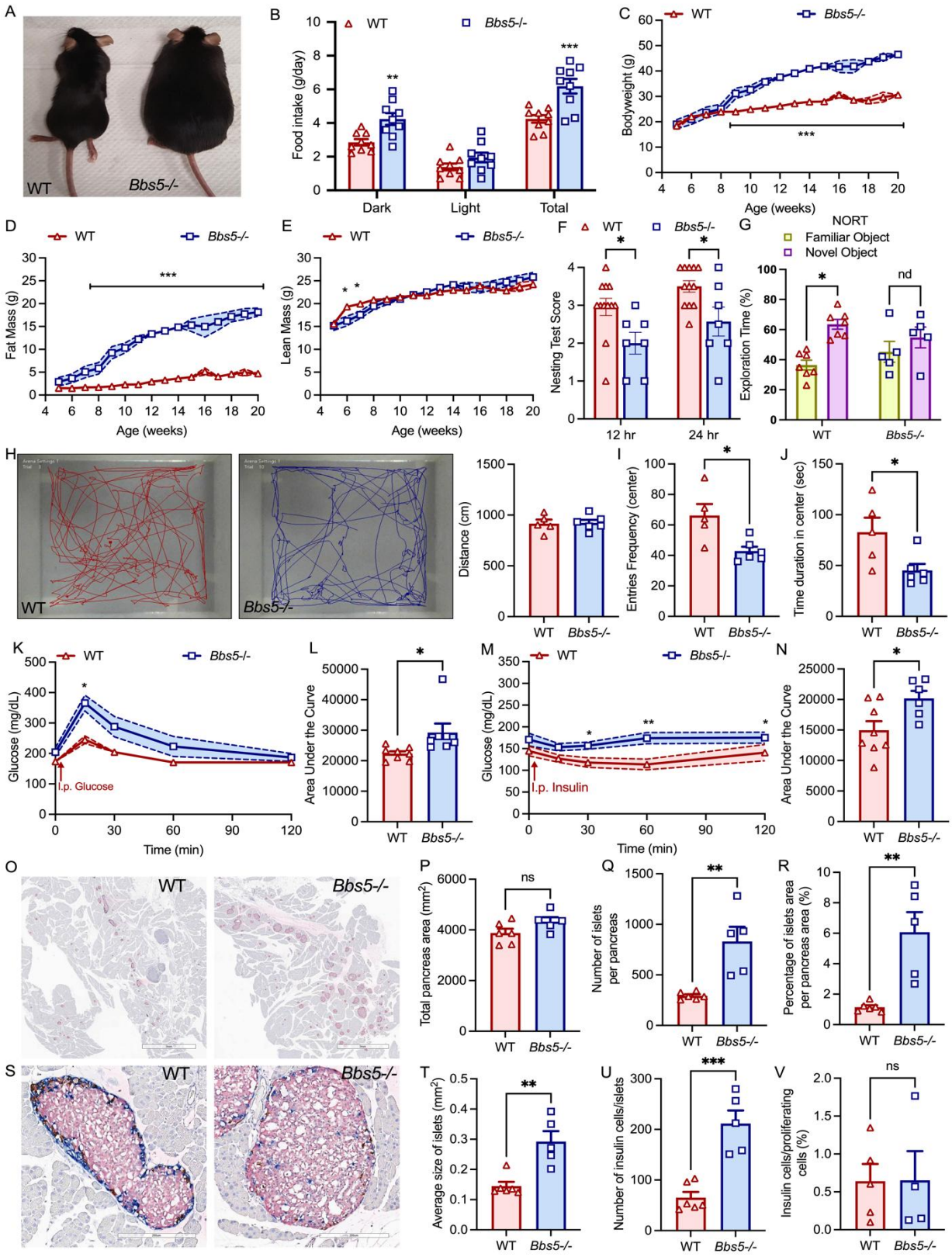

Figure. 1| Adult *Bbs5*-null mice are morbidly obese, hyperphagic, glucose intolerant, and have behavioral and learning impairments. A, Representative image of 12-weeks-old *ad libitum* chow-fed C57BL/6J wildtype (WT) and Bardet Biedl Syndrome 5 gene knockout (*Bbs5*-/-) male mice. **B**, Average cumulative daily *ad libitum* food intake during 12-hour dark and light, and 24-hour periods in 10-18-weeks-old mice (n= 9 per group). **C-F**, Weekly body weight (**C**), fat mass (**D**), and lean mass (**E**) during development in 5-20-weeks-old male mice (n= 5-12 per group). **F,** Nest building score after 12 and 24 hours upon providing cotton-pressed nestlets in 12-18-weeks-old mice (n= 7-12 per group). **G**, Percent exploration time with familiar or novel objects in Novel Object Recognition Paradigm (n= 5- 8 per group). **H**, Representative traces of WT and *Bbs5*-/- mice respectively during 5-min open field test. **H-J**, Distance traveled (**H**), number of entries (**I**), and time duration in the center (**J**) in 14-18-weeks-old mice (n= 6 per group). **K-L**, Intraperitoneal glucose tolerance (**K**) and area under the curve (**I**) in 11-18-weeks-old mice (n= 6-8 per group). **M-N**, insulin tolerance (**M**) and area under the curve (**N**) in 11-18-weeks-old mice (n= 6-8 per group). **O-V**, Representative images of islet immunohistochemistry for insulin, glucagon, and somatostatin staining from pancreas sections (**O**, scale bars: 3mm). Quantitative analyses of total pancreas area (**P**), number of islets (**Q**), percent islet area (**R**), higher magnification images showing a normal distribution of central beta-cells (pink) with peripherally located glucagon (blue) and somatostatin (brown) cells (**S**, scale bars: 200μm), average islet size (**T**), number of insulin cells per islet (**U**), and percent insulin cells per proliferating cells (**V**) of 16-18-weeks-old mice (n= 5-6 per group). Data in **B-G, K** and **M** were analyzed using repeated measures two-way analysis of variance (ANOVA) with Benjamini, Krieger, and

Yekutieli post hoc test (FDR = 0.05) to compare individual time points. Data in **H-J, L, N, P-R** and **T-V** were analyzed using Student's two-sided, two-tailed *t*-test. Data are mean ± s.e.m. from chow-fed WT and *Bbs5*-/- male mice; ns, not significant; **P*<0.05; ***P*<0.01; ****P*<0.001.

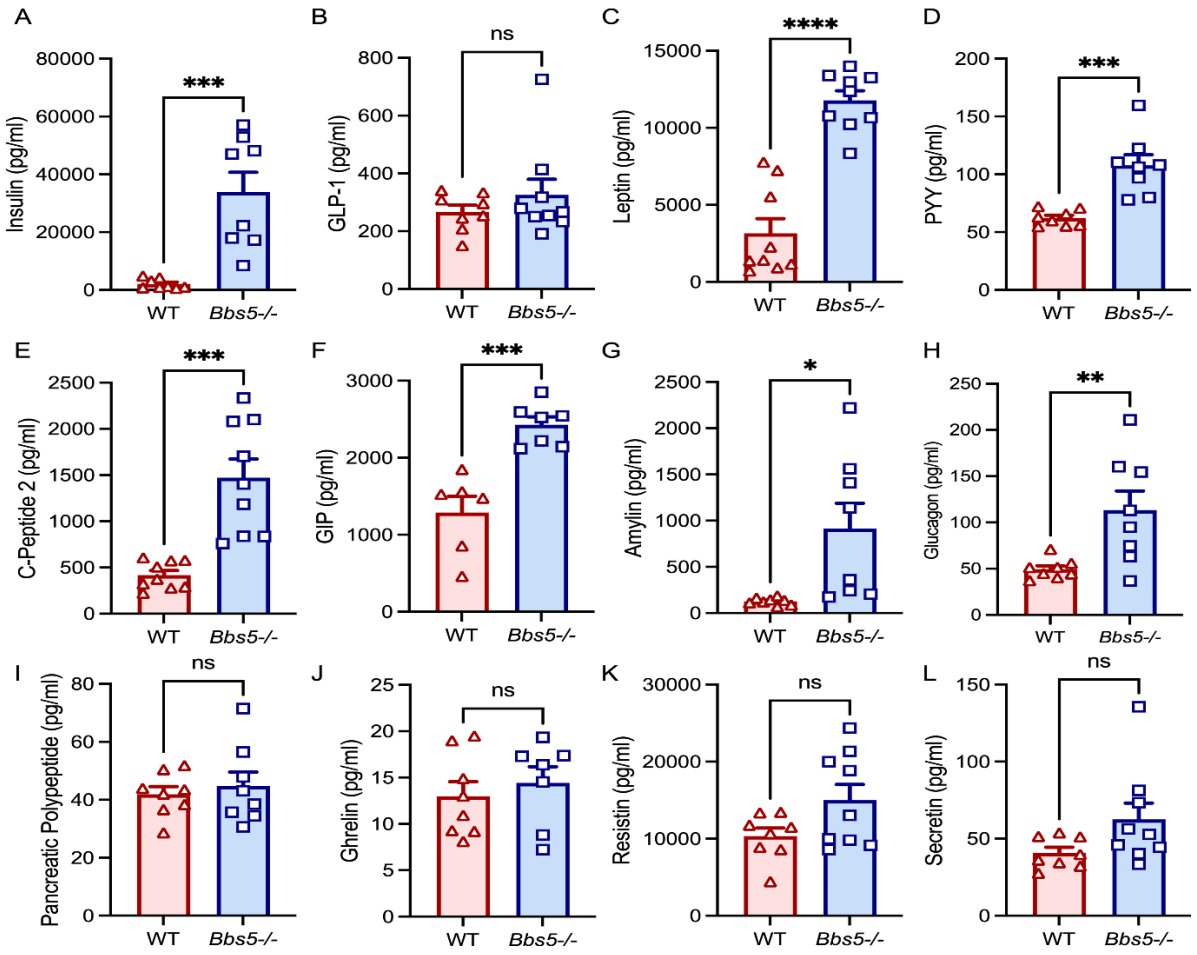

Figure. 2| Adult *Bbs5*-null mice have dysregulated plasma levels of circulating metabolic hormones. A-L, Plasma concentrations of insulin (**A**), glucagon-like peptide-1 (GLP-1, active) (**B**), leptin (**C**), peptide YY (PYY) (**D**), C-peptide 2 (**E**), glucose-dependent insulinotropic polypeptide (GIP, total) (**F**), amylin (active) (**G**), glucagon (**H**), pancreatic polypeptide (PP) (**I**), ghrelin (**J**), Resistin (**K**) and Secretin (**L**) in 15-22 weeks-old *ad libitum* chow-fed C57BL/6J wildtype (WT) and Bardet Biedl Syndrome 5 gene knockout (*Bbs5*-/-) male and female mice (n= 9 per strain). Data in **A-L** were analyzed using Student's two-sided, two-tailed *t*-test. Data are mean ± s.e.m. from WT and *Bbs5*-/- mice; ns, not significant; **P*<0.05; ***P*<0.01; ****P*<0.001; *****P*<0.0001.

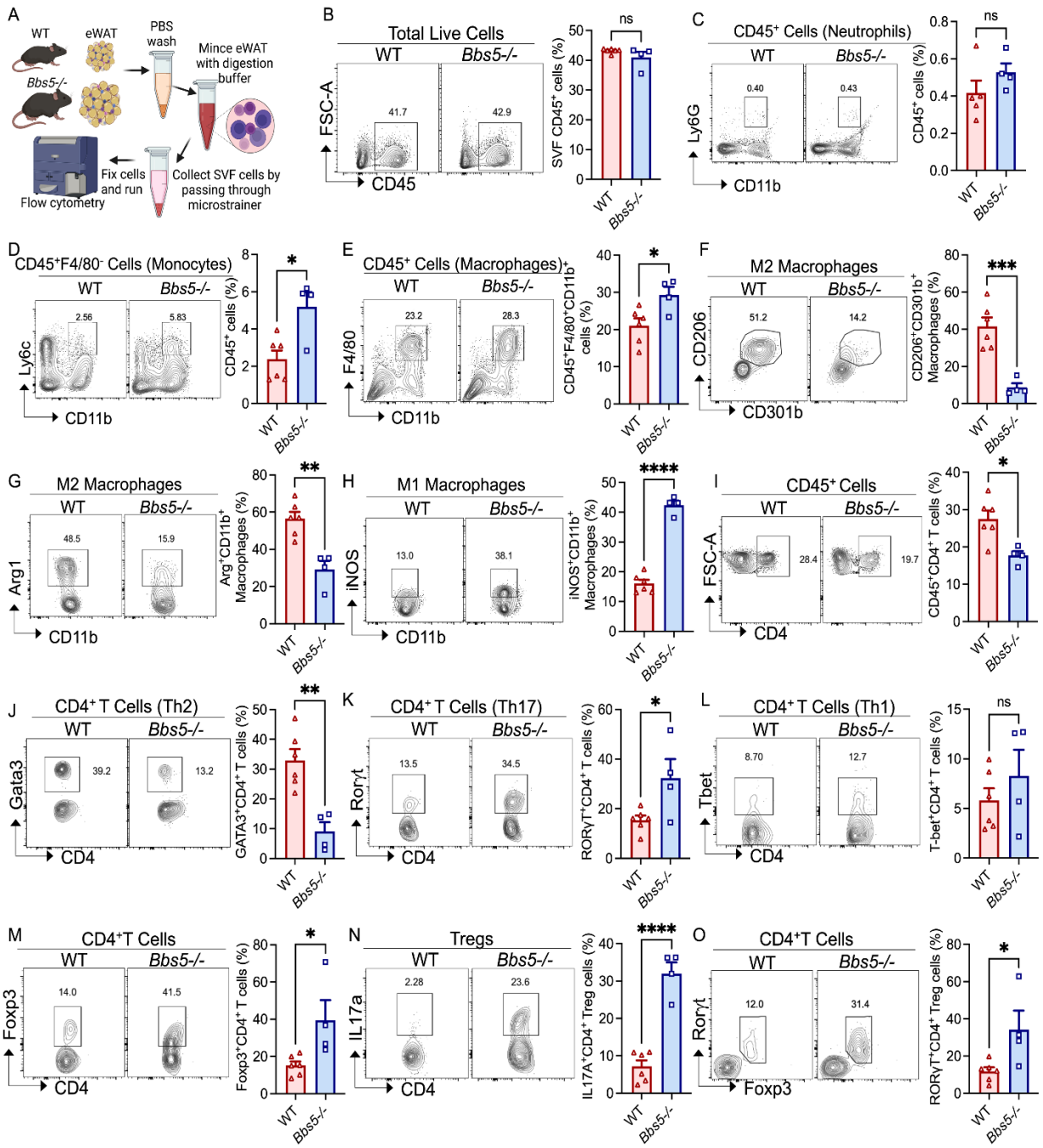

Figure. 3| Adult *Bbs5* null mice have proinflammatory white adipose immunophenotype. A, Schematic workflow diagram of the isolation of immune cells in the stromal vascular fraction (SVF) of epididymal white adipose tissue (eWAT) from WT and *Bbs5*-/- male mice by flow cytometry. **B-O**, Flow cytometry analysis of CD45$^+$ cells

(**B**), neutrophils (**C**), Ly6C^{hi} monocytes (**D**), total macrophages (**E**), CD206^{+}CD301b^{+} M2 macrophages (**F**), Arg^{+} M2 macrophages (**G**), iNOS^{+} M1 macrophages (**H**), CD45^{+}CD4^{+} T cells (**I**), Gata3 Th2 cells (**J**), Rorγt Th17 cells (**K**), Tbet Th1 cells (**L**), Foxp3^{+} Tregs (**M**), IL17^{+} Tregs (**N**), Rorγt^{+}Foxp3^{+} Tregs (**O**) in eWAT of 18-22 weeks old WT and *Bbs5*-/- male mice (n= 4-6 per group). Data are representative of two independent experiments. Data in **B-O** were analyzed using Student's two-sided, two-tailed *t*-test. Data are mean ± s.e.m. from WT and *Bbs5*-/- male mice; ns, not significant; **P*<0.05; ***P*<0.01; ****P*<0.001; *****P*<0.0001.

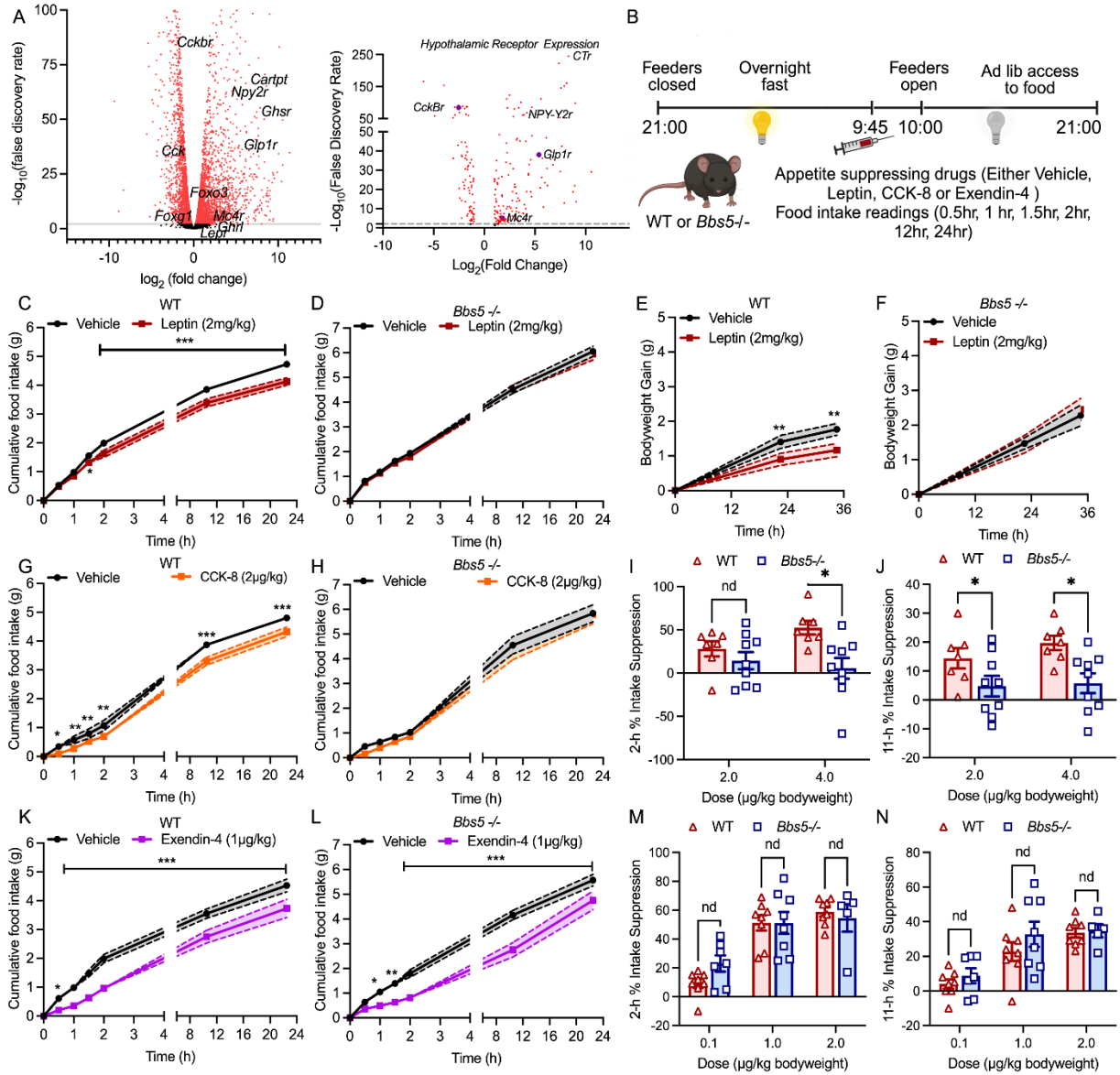

Figure. 4| Hypothalamic RNA transcriptomics predicts leptin and cholecystokinin resistance but retained glucagon-like peptide-1 response in *Bbs5* null male mice. **A**, Volcano plot of differential expression changes, plotting the log fold change of receptors in the hypothalamus between 12-week-old WT and *Bbs5*-/- male mice (n=2-3 per group). Red dots are significant, black are non-significant. **B**, Schematic experimental design to determine anorexigenic effects of leptin, cholecystokinin (CCK-8), and glucagon-like peptide-1 receptor agonist, exendin-4 in overnight fasted WT and

Bbs5-/- male mice. **C-D**, the effect of intraperitoneal leptin (red, 2 mg/kg bodyweight) or vehicle (black) injection on cumulative *ad libitum* food intake in WT (**c**) and *Bbs5*-/- mice (**D**) over 24 hours in 12-18-weeks-old male mice (n= 9 per group). **E-F**, body weight gain in WT (**E**) and *Bbs5*-/- (**F**) at 24- and 36-hour after leptin injections. **G-H**, the effect of intraperitoneal cholecystokinin (CCK-8, orange, 2 μg/kg bodyweight) or vehicle (black) injection on cumulative *ad libitum* food intake in WT (**G**) and *Bbs5*-/- mice (**H**) over 24 hours in 12-18-weeks-old male mice (n= 7-9 per group). **I-J** Food intake suppression relative to saline after 2-hour (**I**) or 11-hour (**J**) in 12-18-weeks-old male WT and *Bbs5*-/- mice following CCK-8 (2 or 4 μg/kg bodyweight) (n= 7-9 per group). **K-L**, the effect of intraperitoneal exendin-4 (GLP-1 agonist, purple, 1 μg/kg bodyweight) or vehicle (black) injection on cumulative *ad libitum* food intake in WT (**K**) and *Bbs5*-/- mice (**L**) over 24 hours in 12-18-weeks-old male mice (n= 8 per group). **M-N**, Food intake suppression relative to saline after 2-hour (**M**) or 11-hour (**N**) in 12-18-weeks-old male WT and *Bbs5*-/- mice following Exendin-4 (0.1 or 1 or 2 μg/kg bodyweight) injection (n= 8 per group). Data in **C-N** were analyzed using repeated measures two-way analysis of variance (ANOVA) with Benjamini, Krieger, and Yekutieli post hoc test (FDR = 0.05) to compare individual time points. Data are mean ± s.e.m. from chow-fed WT (vehicle or drug treated) and *Bbs5*-/- (vehicle or drug treated) male mice; nd, no discovery; **P*<0.05; ***P*<0.01; ****P*<0.001.

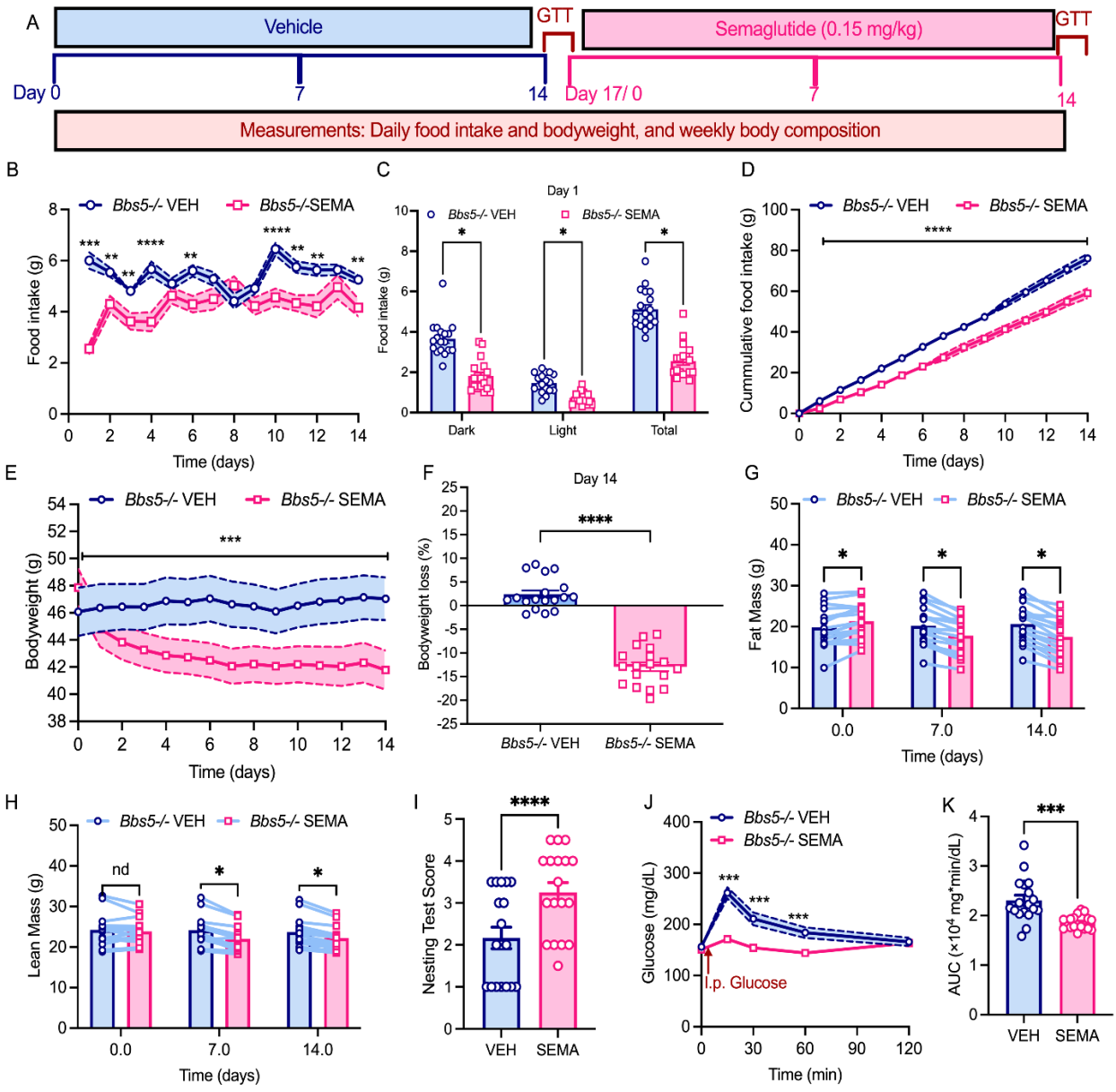

Figure. 5| Glucagon-like peptide-1R agonist (Semaglutide) promotes hypophagia-induced weight loss and improves nesting behavior and glucose tolerance in adult *Bbs5* null mice. A, Schematic diagram of study timeline where obese *ad libitum* chow-fed *Bbs5*-/- mice received daily subcutaneous injections of vehicle (blue) for 14 days followed by semaglutide (pink, 0.15 mg/bodyweight) for 14 days and observed for changes in feeding, body composition, nest building behavior, and glucose tolerance.

The data in **B-K** are from 19-30-weeks-old *Bbs5*-/- mice (n=18 includes 6 males and 12 females). **B-D,** changes in *ad libitum* chow intake daily over 24 hours (**B**), average cumulative intake during 12-hour dark and light, and 24-hour periods (**C**), and average cumulative daily food intake during 14 days of vehicle or semaglutide therapy (**D**). **E-H,** average daily changes in body weight (**E**), average percent weight loss (**F**), weekly changes in fat mass (**G**), and lean mass (**H**) after semaglutide therapy. **I,** Nesting score after 12 and 24 hours upon providing cotton-pressed nestlet before and after semaglutide therapy. **J-K**, Intraperitoneal glucose tolerance (**J**), and area under the curve (**K**) before and after semaglutide therapy.

Data in **B-K** were analyzed using Student's two-sided, two-tailed t-test or repeated measures two-way analysis of variance (ANOVA) with Benjamini, Krieger, and Yekutieli post hoc test (FDR = 0.05) to compare individual time points. Data are mean ± s.e.m. from vehicle or drug-treated mice; *P<0.05; **P<0.01.

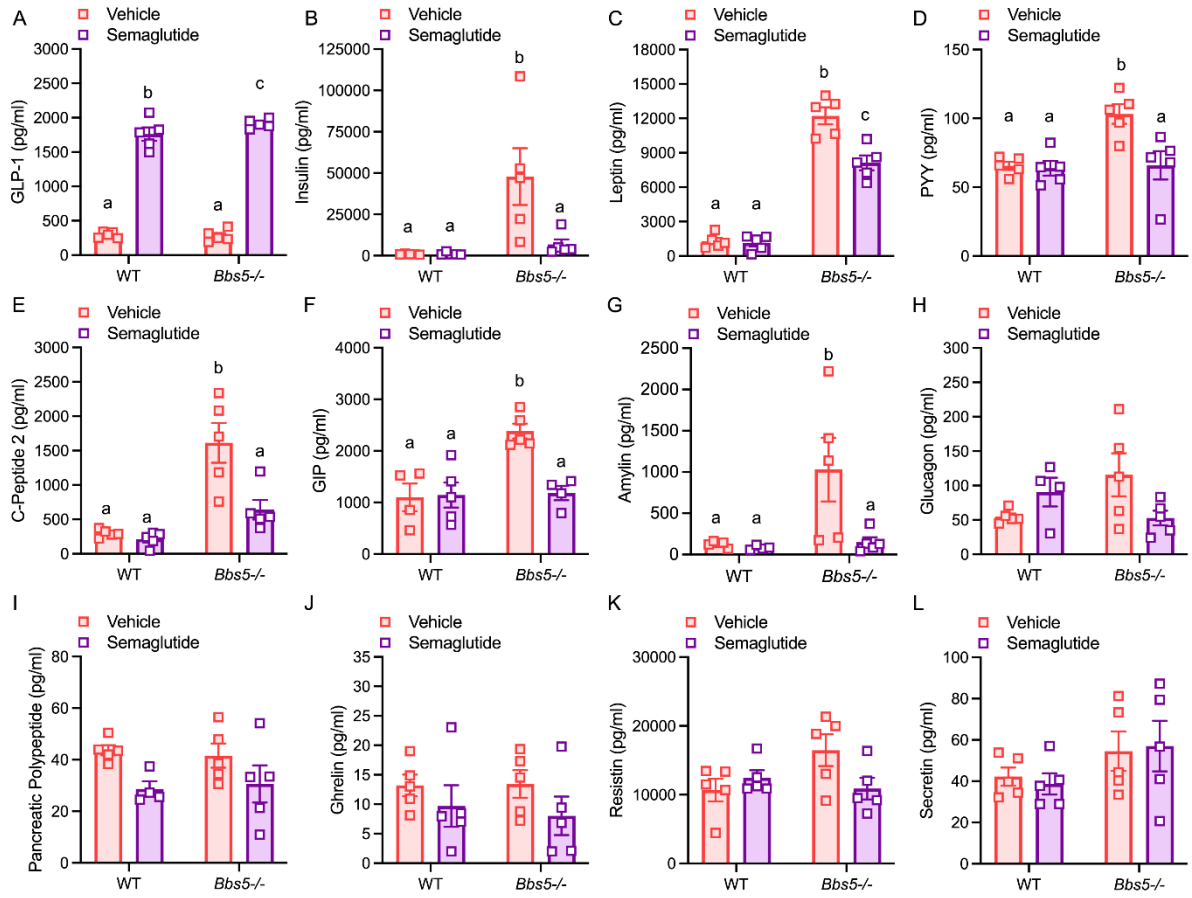

Figure. 6| Semaglutide treatment improves dysregulated plasma levels of circulating metabolic hormones in adult *Bbs5*-null mice. A-L, Plasma concentrations of glucagon-like peptide-1 (GLP-1, active) (**A**), insulin (**B**), leptin (**C**), peptide YY (PYY) (**D**), C-peptide 2 (**E**), glucose-dependent insulinotropic polypeptide (GIP, total) (**F**), amylin (**G**), glucagon (**H**), pancreatic polypeptide (PP) (**I**), ghrelin (**J**), Resistin (**K**) and Secretin (**L**) in 22-28 weeks-old *ad libitum* chow-fed C57BL/6J wildtype (WT) and Bardet Biedl Syndrome 5 gene knockout (*Bbs5*-/-) female mice (n= 5 per group) before and after semaglutide therapy. Data in **A-L** were analyzed using a two-way analysis of variance (ANOVA) with Benjamini, Krieger, and Yekutieli post hoc test

(FDR = 0.05) to compare individual time points. Data are mean ± s.e.m. from WT and *Bbs5*-/- mice; means with no letters in common are significantly different ($P < 0.05$).